An Energy-Efficient MU-MIMO and IRS BackCom Symbiotic Radio Network Resource Allocation

Derek Kwaku Pobi Asiedu, Samuel Menanor, Mustapha Benjillali, Kyoung-Jae Lee, Ji-Hoon Yun, Samir Saoudi

An Energy-Efficient MU-MIMO and IRS BackCom Symbiotic Radio Network Resource Allocation

Derek Asiedu*, Samuel Menanor†, Mustapha Benjillali‡*, Kyoung-Jae Lee†, Ji-Hoon Yun§, and Samir Saoudi*
*IMT-Atlantique, Lab-STICC, Brest, France. Emails: kwakupobi@ieee.org, and samir.saoudi@imt-atlantique.fr
†Department of Electronic Engineering, HBNU, Daejeon, South Korea. Email: {smenanor,kyoungjae}@{edu.}hanbat.ac.kr
‡Communication Systems Department, INPT, Rabat, Morocco. Email: benjillali@ieee.org
§Department of Electrical and Information Engineering, SeoulTech, Seoul, South Korea. Email: jhyun@seoultech.ac.kr

***Abstract*—Symbiotic radio networks (SRN) have gained traction for efficient spectrum usage in wireless communication Internet-of-Things networks (IoTNs) applications. Furthermore, the efficient use of energy resources under energy-efficient communication is rising in IoTNs to satisfy and attain the United Nations' sustainable development goals on sustainable and renewable energy usage. Hence, this work focuses on energy and spectrum efficient usage through renewable radio frequency (RF) energy harvesting (EH) backscatter (BC) communication (BackCom) and SRN between a secondary network sensor-equipped EH intelligent reflective surface BC and a primary network base station to multiple user equipment using multiple access communication. This work focuses on resource allocation optimization to maximize the system energy-efficiency quality-of-service for the SRN. The superiority of the proposed scheme over existing benchmark schemes is also presented in this work.**

***Index Terms*—Energy-efficiency (EE), backscatter, energy harvesting (EH), symbiotic radio, intelligent reflective surfaces (IRS).**

I. Introduction

With the advent of Internet-of-Things Networks (IoTNs) and the further evolution of wireless communication networks, there is a demand for better network speeds, low latency, and high network reliability for end-users (consumers), to mention a few quality-of-service (QoS) needs [1]–[3]. However, with these consumer demands coupled with the new set of sustainable development goals (SDGs) outlined by the United Nations, consumers and the public are geared towards usage and support of telecommunication industries using efficient and sustainable resources. Hence, ongoing industry and academic researches into next-generation wireless communication technologies are focusing on energy- and spectrum-efficient and sustainable usage through new technology development [2], [4]. To this end, significant research into wireless communication techniques for energy and spectrum efficient usage has resulted in new technologies such as spectrum sharing through cognitive/symbiotic radio networks (SRNs), and renewable/sustainable energy usage through radio frequency (RF) energy harvesting (EH), respectively [1], [5].

This work is funded by the Institut Carnot Télécom et Société Numérique, France, under project MacLeRIS. K.-J. Lee's and S. Menanor's work was supported in part by the Institute of Information & Communications Technology Planning & Evaluation (IITP), South Korea grant through Korea Government (MSIT) under Grants 2021-0-00841 and IITP-2024-RS-2022-00156212. J-H Yun's work was financially supported in part by the Basic Science Research Program through the National Research Foundation of Korea (NRF) funded by the Ministry of Education under Grant NRF-2019R1A6A1A03032119.

TABLE I
SRN WITH IRS RELATED WORKS COMPARISON.

Reference	Optimized	Multi-user	Multi-IRS	EH	PN/SN
[5]/ [4]	EE	✘	✘	✔	SN
[7]	EE	✘	✘	✘	PN+SN
[8]/ [9]	BER/EE	✘	✘	✘	SN
[2]	Sum-rate	✔	✔	✘	PN+SN
This work	EE	✔	✔	✔	PN+SN

Spectrum efficient usage through spectrum sharing in SRN is accomplished through several sub-networks (e.g., primary (PN), secondary (SN), and tertiary (TN) networks) sharing the same spectrum resource [1]. The SRN efficient spectrum usage is accompanied by inter-network and inter-device data transfer interference, which can be mitigated using successive interference cancellation (SIC), and/or expected device throughput or interference constraints considerations [1], [2], [5]. SRN has been combined with assistive technologies such as intelligent reflective surface (IRS) to improve network coverage and throughput through spatial diversity. Another SRN application is the combination of PN multi-user multi-access techniques (e.g., NOMA, and RSMA) and SN backscatter (BC) multi-tag and multi-IRS communication [2], [4].

RF EH is accomplished either by the simultaneous and/or the concurrent transmission of power and information signals to a receiver [3], [6]. In addition to studying EH techniques, EH models have been proposed, which consist of the linear (L-EH) and nonlinear (NL-EH) (e.g., threshold, sigmoid, and simple rectifier EH models) [3], [6]. RF EH has been extended to SRN-IRS for efficient energy utilization amongst network devices to reduce the strain on their base power.

EH IRS-assisted SRN research has also covered QoS studies on system analysis and maximization (sum-rate, EH, energy-efficiency (EE) and spectrum-efficiency (SE)) [2], [4], [5], [7]–[9]. These studies however considered the simple L-EH models [4], [5] and not the NL-EH [3], [6]. It is therefore prudent to consider the more realistic NL-EH simple rectifier model in EH IRS-assisted SRN research. Concerning the network architecture, the generalized case of IRS-assisted SRN has been studied for SR maximization and not other QoS

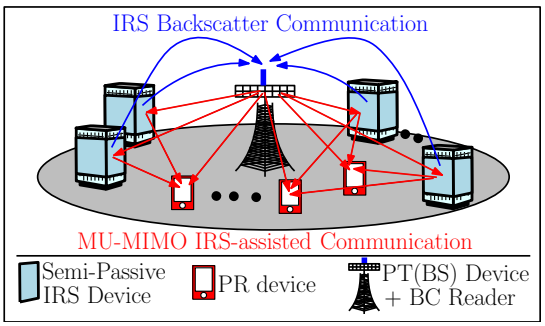

Fig. 1. MU-MISO with integrated IRS BC SRN.

metric. Also, massive primary transmitter (PT) large antenna for improved spatial diversity and multiple primary receivers (PRs) for improved spectrum usage are not covered in current research. Finally, the general case and influence of multiple secondary transmitters (STs) with sensor-equipped IRS BC devices within an SRN to improve coverage and throughput must be studied. It is therefore critical to consider these to take full advantage of network resources and novel technologies.

To this end, this paper covers research on optimal resource allocation (i.e., PT power and ST reflection coefficient) for an EH IRS-assisted SRN to maximize the system EE QoS. Unlike the current literature and as shown in Table I, this work focuses on multiple PRs and STs, extends the simple rectifier NL-EH model to multi-stage NL-EH model, as well as EE.

II. System Models and Problem Formulations

We consider the SRN IoT model shown in Fig. 1, where the PN consists of a N_S multi-antenna source (PT(D_S)) communicating with L single antenna PRs(D_l). The SN consists of K senor equipped (semi-passive) IRS devices (STs(T_k)) with M_k reflective elements. Each IRS has an embedded EH sensor for critical environmental data monitoring (e.gs. humidity, temperature, structure failure, etc). The sensor data are transferred using wireless powered BC communication (BackCom). The IRSs transfer the collected data to a centralized secondary receiver (SR(T_R)) BC reader. The mutually beneficial symbiotic relationship between the PN and SN exists as follows. The SN network benefits from the PN by accessing its spectrum and using the PN RF for its BC technique implementation and RF EH. The PN benefits from the IRS-assisted communication via the IRS BC from the STs to PRs transmission improving the PN spatial diversity. The data signals flow is as follows.

A. PN and SN Data Transmissions

The generalized received signals at D_l and T_R is defined as

$$\mathbf{y}_{z_1,z_2} = \mathbf{n}_{z_2} + \underbrace{\sum_{j=1}^{L} \mathbf{h}_{S,z_2}^H \mathbf{v}_{S,j}\mathbf{x}_{S,j}}_{\text{PN direct-link signals}} + \underbrace{\sum_{k=1}^{K} \mathbf{G}_{S,k}^H \Big(\sum_{l=1}^{L} \mathbf{v}_{S,l}\mathbf{x}_{S,l}^H \mathbf{x}_k\Big) \boldsymbol{\Theta}_k^{\frac{1}{2}H} \mathbf{g}_{k,z_2}}_{\text{Multi-IRS BC signals (SN IRS data + PN data)}}, \quad (1)$$

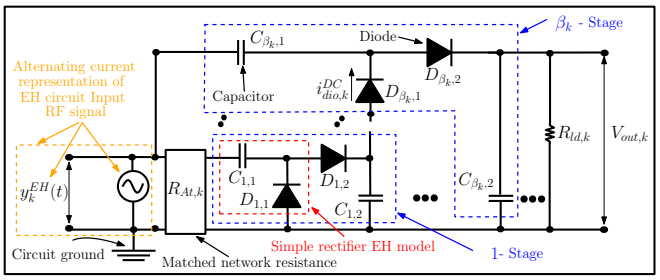

Fig. 2. EH circuit schematic diagram.

where $(z_1, z_2) \in \{(S,l),(k,R)\}$, $\mathbf{h}_{S,z_2}$ and $\mathbf{g}_{k,z_2}$ are respectively the PT and IRS$_k$ channels to either PR ($z_2 = l$) or SR ($z_2 = R$). $\mathbf{v}_{S,l}$ is the PT to PR l beamforming vector. $\boldsymbol{\Theta}_k$ is IRS$_k$ reflection coefficient diagonal matrix. $\mathbf{x}_{S,l}$ and $\mathbf{x}_k$ are the PR$_l$ and the IRS data, respectively. The signal-to-interference-noise ratio (SINR) for D_l and T_k data at T_R are deduced as

$$\hat{\gamma}_{z_1,z_2} = A_{z_1,z_2}/[B_{z_1,z_2} + C_{z_1,z_2} + D_{z_1,z_2} + \sigma_{z_2}^2], \quad (2)$$

where $A_{S,l} = |\mathbf{h}_{S,l}^H \mathbf{v}_{S,l}|^2 + \sum_{k=1}^{K} |\mathbf{g}_{k,l}^H \boldsymbol{\Theta}_k^{\frac{1}{2}} \mathbf{G}_{S,k} \mathbf{v}_{S,l}|^2$, $A_{k,R} = \sum_{l=1}^{L} |\mathbf{g}_{k,R}^H \boldsymbol{\Theta}_k^{\frac{1}{2}} \mathbf{G}_{S,k} \mathbf{v}_{S,l}|^2$, $C_{k,R} = \sum_{l=1}^{L} |\mathbf{h}_{S,R}^H \mathbf{v}_{S,l}|^2$, $C_{S,l} = \sum_{j=1}^{L} \sum_{k=1}^{K} |\mathbf{g}_{k,l}^H \boldsymbol{\Theta}_k^{\frac{1}{2}} \mathbf{G}_{S,k} \mathbf{v}_{S,j}|^2$, $D_{S,l} = 0$, $B_{S,l} = \sum_{j \neq l}^{L} |\mathbf{h}_{S,l}^H \mathbf{v}_{S,j}|^2 + \sum_{j \neq l}^{L} \sum_{k=1}^{K} |\mathbf{g}_{k,l}^H \boldsymbol{\Theta}_k^{\frac{1}{2}} \mathbf{G}_{S,k} \mathbf{v}_{S,j}|^2$, $D_{k,R} = \sum_{j=1}^{K} \sum_{l=1}^{L} |\mathbf{g}_{k,R}^H \boldsymbol{\Theta}_j^{\frac{1}{2}} \mathbf{G}_{S,k} \mathbf{v}_{S,l}|^2$, and $B_{k,R} = \sum_{j \neq k}^{K} \sum_{l=1}^{L} |\mathbf{g}_{k,R}^H \boldsymbol{\Theta}_j^{\frac{1}{2}} \mathbf{G}_{S,k} \mathbf{v}_{S,l}|^2$. $A_{S,l}$, $B_{S,l}$, $C_{S,l}$, $A_{k,R}$, $B_{k,R}$, $C_{k,R}$ and $D_{k,R}$ are the PR$_l$ desired signal, the set of PR$_j$ interference signals, the set of ST$_k$ backscattered signals, the IRS$_k$ desired signal, the set of IRS$_j$ backscattered interference signals, all PN direct links interference signals and all PN backscattered data interference signals, respectively.

B. IRS Energy Harvesting

The energy harvested by T_k based on the multi-stage EH model in Fig. 2 for backscattering is deduced as [6], [10]

$$Q_k \approx \frac{\beta_k^2 R_{At,k}^2 \sum_{l=1}^{L} \hat{v}_{k,l}}{4 R_{ld,k} \alpha_k^2 V_{T,k}^2} + \frac{\beta_k^2 R_{At,k}^3 \sum_{l=1}^{L} \bar{v}_{k,l}}{32 R_{ld,k} \alpha_k^4 V_{T,k}^4} + \frac{\beta_k^2 R_{At,k}^4 \sum_{l=1}^{L} \tilde{v}_{k,l}}{1024 R_{ld,k} \alpha_k^6 V_{T,k}^6}, \quad (3)$$

where $\hat{v}_{k,l} = |(\mathbf{i} - \boldsymbol{\theta}_k)^{\frac{1}{2}H} \mathbf{G}_{S,k} \mathbf{v}_{S,l}|^4$, $\bar{v}_{k,l} = \hat{v}_{k,l}^{\frac{3}{2}}$, $\tilde{v}_{k,l} = \hat{v}_{k,l}^2$. β_k is the number of voltage multiplier stages in the IRS EH circuit, $\mathbf{i}$ is vector of ones, and $\boldsymbol{\theta}_k$ is a vector of IRS$_k$ reflection coefficients. $R_{At,k}$, $R_{ld,k}$, α_k and $V_{T,k}$ are ST l antenna impedance load, power system load, ideality factor and diode thermal voltage, respectively [6], [10].

C. System Behavior and Deductions

The influence of the SRN resources $(P_T, P_{\text{cir},k})$, antenna structure (N_S, M_k) and devices (L, K) has on the SRN are discussed next. For the analysis, it is assumed all IRS have the same number of reflective elements M, and all inter-node expectation components unrelated to the network components listed above are equal and represented by $\mathbb{E}_{SL}$,

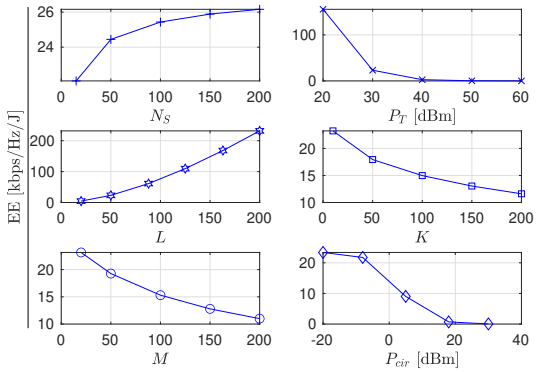

Fig. 3. EE MRT analytical behavior.

$\mathbb{E}_{SR}$, $\mathbb{E}_{SKL}$, and $\mathbb{E}_{SKR}$. Rician channel fading is adopted and the expectation derivations are in Appendix A. The deductions are illustrated in Fig. 3 and summarized as follows.

- The EE rises to $(\bar{A}_1+\bar{A}_2)/(P_T+KP_{\text{cir}})$, as $N_S\to\infty$.
- The EE falls to $\bar{A}/P_T\approx 0$, as $P_T\to\infty$.
- The EE approaches infinity (∞), as $L\to\infty$.
- The EE falls to $\hat{A}_2/KP_{\text{cir}}\approx 0$, as $K\to\infty$.
- The EE falls to $(\hat{A}_1+\hat{A}_2)/(P_T+KP_{\text{cir}})$, as $M\to\infty$.
- The EE falls to $(\bar{A}_1+\bar{A}_2)/KP_{\text{cir}}\approx 0$, as $P_{\text{cir}}\to\infty$.

Where, $\bar{A}_1 = L\log_2\left(1+\frac{\mathbb{E}_{SL}+0.5KM^3\mathbb{E}_{SKL}}{(L-1)\mathbb{E}_{SL}+0.5KM^3\mathbb{E}_{SKL}(2L-1)}\right)$, $\bar{A}_2 = K\log_2\left(1+\frac{0.5M^3\mathbb{E}_{SKR}}{0.5M^3\mathbb{E}_{SKR}(2K-1)+\mathbb{E}_{SR}}\right)$ and $\hat{A}_1 = L\log_2(1+1/(2L-1))$, $\hat{A}_2 = K\log_2(1+1/(2K-1))$. From the propositions, the following inferences can be made.

- Large N_s is desired, hence, massive antenna PT (massive MIMO) can be deployed in an SRN.
- It is redundant for the PT to use high P_T. Therefore, P_T must be well regulated during data transfer.
- It is advantageous to use low P_T to serve a larger L PRs, and simultaneously excite (Backscatter) fewer K IRSs.
- It is beneficial if the K IRSs have a moderate number of M deployed, this translates to the amount of P_{cir} consumed by operating the IRS (better energy efficiency).

After deployment, N_s, M and P_{cir} cannot be changed. However, after deployment and during information transfer, the SRN can decide the resource allocation $(P_T,\boldsymbol{\theta})$ and the trade-off number of PRs (L) and STs (K) allowed to exchange information within a coherence time to make their interaction mutually beneficial. Therefore, the PT transmit power allocation and the reflection co-efficient of the IRSs must be optimized. The number of PRs and STs communicating within a coherence time must be determined to promote the symbiotic relationship between the PN and SN. It is difficult to determine (optimal) a trade-off value between L and K to maximize the EE. Hence, falling on the EE equivalency based on in [2], with K or L defined, the other can be approximated from

$$L\approx[1/\theta M^3\mathbb{E}_{SKR}(\mathbb{E}_{SL}+2\mathbb{E}_{SKL})][\mathbb{E}_{SL}+\theta KM^3\mathbb{E}_{SKL} + (\mathbb{E}_{SL}+\theta KM^3\mathbb{E}_{SKL})(\mathbb{E}_{SR}+\theta(2K-1)M^3\mathbb{E}_{SKR})] \tag{4}$$

or as the root of the equation[1]

$$K^2[2\theta^2M^6\mathbb{E}_{SKR}\mathbb{E}_{SKL}]+\mathbb{E}_{SR}[\mathbb{E}_{SL}-\theta M^3\mathbb{E}_{SKR}] + K[\theta M^3(\mathbb{E}_{SKR}(2\mathbb{E}_{SL}-\theta M^3\mathbb{E}_{SKL}) + \mathbb{E}_{SKL}(\mathbb{E}_{SR}+\theta M^3\mathbb{E}_{SKR}(2L-1)))]. \tag{5}$$

D. Optimization Problem Formulation

This work focuses on EE maximization with IRS reflection co-efficient ($\{\boldsymbol{\Theta}_k\}_{k=1}^K$) and PT beamforming vector ($\{\mathbf{v}_{S,l}\}_{l=1}^L$) optimization. The associated constraints are $\|\boldsymbol{\Theta}_k\|^2\le M_k$, and $\sum_{l=1}^L\|\mathbf{v}_{S,l}\|^2\le P_T$, where P_T is the PT transmit power. The EE problem is defined as[2]

$$\underset{\{\mathbf{v}_{S,l}\}_{l=1}^L,\{\boldsymbol{\Theta}_k\}_{k=1}^K}{\text{maximize}}\ \Pi/\mathcal{E}\ \text{subject to}\ \|\boldsymbol{\Theta}_k^{1/2}\|^2\le M_k,\ \forall k,\ \text{(6a)}$$
$$\sum_{l=1}^L\|\mathbf{v}_{S,l}\|^2\le P_T,\ \text{(6b)}\ Q_k\le P_{cir},\forall k,\ \text{(6c)} \tag{6}$$

where $\Pi=\sum_{l=1}^L\log_2(1+\hat{\gamma}_{S,l})+\sum_{k=1}^K\log_2(1+\hat{\gamma}_{k,R})$, and $\mathcal{E}=\sum_{l=1}^L\|\mathbf{v}_{S,l}\|^2+P_{cir}$. P_{cir} is IRS$_k$ circuit power consumed for data processing and transmission, which is facilitated by the energy harvested, Q_k. Concerning convexity, constraints (6a) and (6b), and $\mathcal{E}$ are quadratic functions and convex in nature with respect to (w.r.t.) their corresponding variables. However, Π is non-convex, therefore, the objective function is non-convex w.r.t. all variables and hard to solve.

III. Proposed Model-Based Optimization Solution

Problem (6) is transformed to a weighted minimum mean square error (WMMSE) problem, and an alternating optimization algorithm proposed to maximize EE. WMMSE is adopted because it is less complex than other methods, requiring multiple-level iterations [11], [12].

A. Sum-rate-to-WMMSE Problem Conversion

Problem (6) is solved by adopting sequential convex optimization tools with fractional programming [11], [12]. This involves a combination of (a) the DinkelBach and dual decomposition methods combined with (b) the WMMSE which converts Problem (6) into a convex optimization problem and makes it easier to determine the EE optimum solution [12].

The Dinkelbach's transformation is derived as

$$\underset{y,\{\mathbf{v}_{S,l}\}_{l=1}^L,\{\boldsymbol{\Theta}_k\}_{k=1}^K}{\text{maximize}}\ \Pi-y\mathcal{E}\ \text{subject to (6a), and (6b),} \tag{7}$$

where $y=\Pi/\mathcal{E}$ is an auxiliary variable. The WMMSE conversion of Π is summarized as follows. The WMMSE filters for the PN and SN are derived as

$$\psi^*_{z_1,z_2}=E_{z_1,z_2}/[A_{z_1,z_2}+B_{z_1,z_2}+C_{z_1,z_2}+D_{z_1,z_2}+\sigma^2_{z_2}], \tag{8}$$

where $E_{S,l}=\mathbf{h}_{S,l}^H\mathbf{v}_{S,l}+\sum_{k=1}^K\mathbf{G}_{S,k}^H\mathbf{v}_{S,l}\boldsymbol{\Theta}_{k,l}^{\frac{1}{2}H}\mathbf{g}_{k,l}$ and $E_{k,R}=\sum_{l=1}^L\mathbf{G}_{S,k}^H\mathbf{v}_{S,l}\boldsymbol{\Theta}_k^{\frac{1}{2}H}\mathbf{g}_{k,R}$, which yields the MSEs defined as

[1]Typically, a few IRSs will be deployed within a network. Hence, all IRSs can transmit, and the L determined, which is less computationally intensive. Fig. 3 unless stated; $\{N_s,P_T,L,K,M,P_{cir}\}=\{25,30,20,10,20,-16\}$

[2]Problem (6) does not include the SN interference and rate constraints to promote PN and SN mutual benefit [2].

Algorithm 1 Model-based EE maximization algorithm

Initialize $\{\mathbf{v}_{S,l}, \mathbf{\Theta}_k\}$ with $\sum_{l=1}^{L} \mathbf{v}_{S,l} \leq P_T, \|\mathbf{\Theta}_k^{\frac{1}{2}}\|^2 \leq M_k$
repeat
  Update $\{\psi_{S,l}, \psi_{k,R}\}$ and $\{\omega_{S,l}, \omega_{k,R}\}$ from (8) and (10)
  Update $\mathbf{v}_{S,l}$ and $\mathbf{\Theta_k}$ from (18), (14), $\forall l$ and , $\forall k$
until EE converges

$\varphi^*_{z_1,z_2} = (A_{z_1,z_2} + B_{z_1,z_2} + C_{z_1,z_2} + \sigma^2_{z_2})^{-1}(B_{z_1,z_2} + C_{z_1,z_2} + \sigma^2_{z_2})$. The MSE to rate relationship is determined as

$$R_{z_1,z_2} = \log_2(\varphi_{z_1,z_2})^{-1}. \tag{9}$$

The weighted MSEs of the PN and SN data are defined as

$$\phi_{z_1,z_2} = \omega_{z_1,z_2}\varphi_{z_1,z_2} - \log_2(\omega_{z_1,z_2}), \tag{10}$$

where $\omega_{S,l}$, and $\omega_{k,R}$ are the assigned MSE weights for the PRs and SR, respectively. The optimal weights are expressed as $\omega_{S,l} = (\varphi_{S,l})^{-1}$ and $\omega_{k,R} = (\varphi_{k,R})^{-1}$ for the PRs and SR, respectively, which implies, $\phi_{S,l} = 1 - R_{S,l}$ and $\phi_{k,R} = 1 - R_{k,R}$. From the sum-rate-to-WMMSE equivalency derivations, the transformed convex WMMSE problem is presented as

$$\underset{\{\mathbf{v}_{S,l}\}_{l=1}^{L}, \{\mathbf{\Theta}_k\}_{k=1}^{K}}{\text{minimize}} \quad \hat{\Pi} - \hat{y}\mathcal{E} \text{ subject to (6a) to (6c)}, \tag{11}$$

where $\hat{\Pi} = \sum_{l=1}^{L} \phi_{S,l} + \sum_{k=1}^{K} \phi_{k,R}$ and $\hat{y} = \hat{\Pi}/\mathcal{E}$.

B. Proposed Model-based Alternating Optimization Solution

The individual variable closed-form solutions for the EE maximization iterative algorithm are summarized as follows. First, $\psi_{S,l}$ and $\psi_{k,R}$ are derived in (8) as $\omega_{S,l} = (\varphi_{S,l})^{-1}$ and $\omega_{k,R} = (\varphi_{k,R})^{-1}$. The optimal $\{\mathbf{v}_{S,l}\}_{l=1}^{L}$ is acquired from

$$\underset{\{\mathbf{v}_{S,l}\}_{l=1}^{L}}{\text{minimize}} \quad \hat{\Pi} - \hat{y}\mathcal{E} \text{ subject to (6a) and (6b)} \tag{12}$$

as $\mathbf{v}_{S,l} = (\mathbf{\Delta}_l)^{-1}\boldsymbol{\delta}_l$ where the components and variables derivations are presented in Appendix B. Algorithm 1 contains the alternating optimization algorithm to maximize the EE.

C. Proposed Algorithm Convergence and Overhead Analysis

The PT has knowledge of all the SRN channel statistics and the complexity of its algorithm implemented centrally is discussed as follows. The algorithm determines the EE for convergence, the PT to PR beamformers ($\{\mathbf{v}_{S,l}\}_{l=1}^{L}$), the ST (IRS) reflection co-efficient ($\{\boldsymbol{\theta}\}_{k=1}^{K}$) and the WMMSE associated variables $(\{\psi_{k,R}, \omega_{k,R}\}_{k=1}^{K}, \{\psi_{S,l}, \omega_{S,l}\}_{l=1}^{L})$. Therefore, the big O computational complexity for executing Algorithm 1 is given as $\mathcal{O}(I[K^3 + L^3 + \log(1/\epsilon)])$, where I represents Algorithm 1 iterations computation, $\log(1/\epsilon)$ is the convergence criterion computation and $K^3 + L^3$ is the arithmetic computation of the various variables. The convergence of Algorithm 1 is shown graphically in the next Section. Now, to reduce the complexity associated with Algorithm 1, traditional linear equal power allocation beamformers (zero-forcing (ZF) and maximum ratio transmission (MRT)) with fixed IRS reflection co-efficient and similar approximate computational complexity of $K + L + \log(1/\epsilon)$ are used as benchmarks and alternate algorithm reduction options.

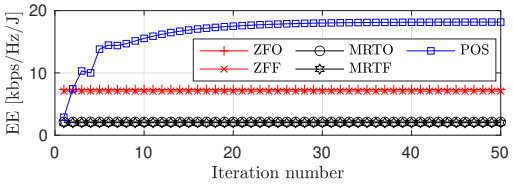

Fig. 4. POS and benchmarks convergence.

IV. Algorithm Evaluation and Discussion

Here the simulation comparison of the proposed optimal scheme ("POS") and benchmark schemes (ZF with optimal $\boldsymbol{\theta}_k$ (ZFO), ZF with fixed $\boldsymbol{\theta}_k = 0.5$ (ZFF), MRT with optimal θ (MRTO), and MRT with fixed $\theta_k = 0.5$ (MRTF)) are presented. The simulation topology is defined as follows. For the topology consisting of high(wall) mounted STs, SR and PT, and ground level PRs, PT is positioned at coordinates $(x_{\text{PT}}, y_{\text{PT}}, z_{\text{PT}}) = (0, 0, 10^2)$m. The SN (STs and SR) and PR devices are randomly distributed within the coordinates $(\{x_{\text{SN}}, y_{\text{SN}}\}, z_{\text{SN}}) \in ([-10^2, 10^2], [10^1, 10^{1.5}])$m and $(\{x_{\text{PR}}, y_{\text{PR}}\}, z_{\text{PR}}) \in ([-10^2, 10^2], [10^0, 10^{0.5}])$m, respectively. The euclidean distance is used to determine the inter-node distances, and the Rician fading channel model is adopted. Each channel geometric attenuation factor is $A_z = 30$dB. The Rician factors and pathloss exponents for the SN interactions are $\{\mu_{s,k}, \mu_{k,l}, \mu_{k,r}\} = 3$ and $\{\zeta_{s,k}, \zeta_{k,l}, \zeta_{k,r}\} = 2.5$, and the PN interactions are $\{\mu_{p,l}, \mu_{s,r}\} = 4$ and $\{\zeta_{p,l}, \zeta_{s,r}\} = 3$. Also, $N_S = 25$, $L = 20$, $K = 4$, $\alpha_k = 1.5$, $\beta_k = 4$, $R_{At,k} = 50\Omega$, $R_{ld,k} = 10^5\Omega$, $V_{T,k} = 25.86$mV, and $P_T = 20$dBm [2], [6].

The convergence of various schemes are shown in Fig. 4. The POS solution is acquired with less than 30 iterations. Also, the benchmarks have constant and lesser EE values with increasing iterations because of the use of closed-form arithmetic solutions in those schemes. Finally, the benchmarks achieve lesser EE values compared to the POS.

Now, the performance of POS in comparison to the benchmark (ZFO, ZFF, MRTO, MRTF) with respect to varying network resources and device architecture are presented in Figs. 5, 6, and 7. From all the figures, the ZFO and ZFF have marginal performance differences. This behavior is also observed for MRTO and MRTF. This observed behavior is due to the PT transmit power equal power allocation assumption in this work. Hence, optimizing the IRS co-efficient in the benchmark schemes has little influence on SRN performance. In terms of overall performance, POS is superior to the benchmarks. Next to POS in performance ranking, the ZF schemes are better than the MRT schemes. Generally, and by observation, the behavior of the plots (POS, ZFO, ZFF, MRTO, and MRTF curves) maintain the patterns discussed in Section II-C. The benefit of POS over the benchmarks lay in its EE high saturation points seen in Figs. 5, 6, and 7. Hence, apart from the P_R and P_{cir} plots, the POS EE saturation values are about $\{150, 50, 80\}$ bps/Hz/J in $\{N_S, K, M_k\}$ plots, respectively.

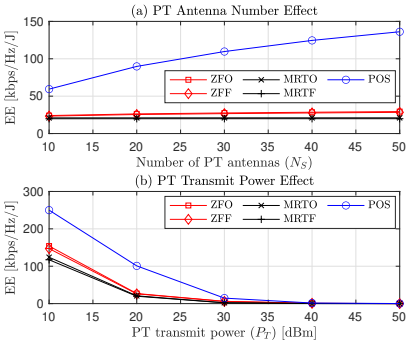

Fig. 5. EE against varying (a) N_S and (b) P_T.

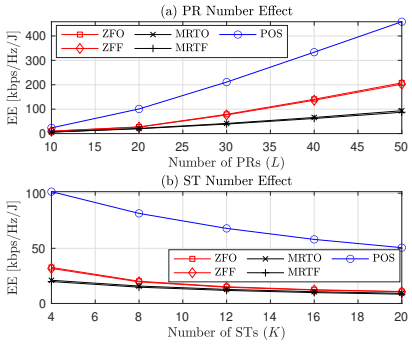

Fig. 6. EE against varying (a) L and (b) K.

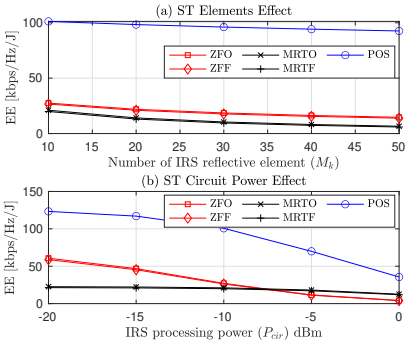

Fig. 7. EE against varying (a) M_k and (b) P_{cir}.

V. Concluding Remarks

This paper tackled the optimal resource allocation for a generalized symbiotic radio network (SRN) consisting of a multiple access primary network (PN) and an energy harvesting (EH) backscatter (BC) communication (BackCom) secondary network (SN). The PN consists of a base station downlink communication with multiple user equipment assisted by multiple EH IRS devices. Simultaneously, the SN consisting of the multiple EH sensor-equipped IRS devices backscatter the sensor data to a backscatter reader. Here, the optimal resource allocation to maximize the SRN energy efficiency is tackled, and an alternating optimization algorithm is proposed. The proposed scheme is compared to benchmarks in simulations. From the simulation, it is shown that the proposed scheme outperforms the benchmark schemes. This work's extensions will offer lower complexity algorithms, considering trade-offs between spectrum and energy efficiency, multi-antenna-equipped receiver devices, and many other possible concerns.

Appendix A
System Analysis Components Derivation

The expectations of Rician fading channel are deduced as

$$\mathbb{E}[\mathbf{h}_{S,z_2}] \approx (\mu_{S,z_2}^{1/2}+\chi_{S,z_2})N_S\left(\frac{A_{S,z_2}\left(\frac{d_{S,z_2}}{d_0}\right)^{-\zeta_{S,z_2}}}{(\mu_{S,z_2}+1)}\right)^{\frac{1}{2}},$$

$$\mathbb{E}[\mathbf{g}_{k,z_2}] \approx (\mu_{k,z_2}^{1/2}+\chi_{k,z_2})M_k\left(\frac{A_{k,z_2}\left(\frac{d_{k,z_2}}{d_0}\right)^{-\zeta_{k,z_2}}}{(\mu_{k,z_2}+1)}\right)^{\frac{1}{2}}, \text{ and}$$

$$\mathbb{E}[\mathbf{G}_{S,k}] \approx (\mu_{S,k}^{1/2}+\chi_{S,k})N_S M_k\left(\frac{A_{S,k}\left(\frac{d_{S,k}}{d_0}\right)^{-\zeta_{S,k}}}{(\mu_{S,k}+1)}\right)^{\frac{1}{2}}, \text{ where}$$

μ_{z_2} represents the Rician factor for each channel, ζ_{z_1,z_2} represents pathloss exponent and all antenna small-scale fading channel components are assumed to be equivalent. In addition, equal power allocation and MRT are assumed for PT transmission, that is, $\mathbb{E}[\mathbf{v}_{S,l}] = \frac{P_T}{L}\mathbb{E}[\mathbf{h}_{S,l}/\|\mathbf{h}_{S,l}\|]$, and the reflection co-efficient is set as 0.5.

Now, the expectations of the SINRs are given as follows. For the PN, the SINR expectation is defined as $\mathbb{E}[\hat{\gamma}_{z_1,z_2}] = \frac{\mathbb{E}[A_{z_1,z_2}]}{\mathbb{E}[B_{z_1,z_2}]+\mathbb{E}[C_{z_1,z_2}]+\mathbb{E}[D_{z_1,z_2}]+1}$, with the various components deduced as follows.

$$\mathbb{E}[A_{S,l}] \approx \frac{P_T}{L}\frac{\left(A_{S,l}\left(\frac{d_{S,l}}{d_0}\right)^{-\zeta_{S,l}}\right)}{(\mu_{S,l}+1)}(\mu_{S,l}^{1/2}+\chi_{S,l})^2N_S^2 + \sum_{k=1}^{K}\frac{0.5M_kP_T}{L}\frac{\left(A_{k,l}A_{S,k}\left(\frac{d_{k,l}}{d_0}\right)^{-\zeta_{k,l}}\left(\frac{d_{S,k}}{d_0}\right)^{-\zeta_{S,k}}\right)}{(\mu_{k,l}+1)(\mu_{S,k}+1)}(\mu_{k,l}^{1/2}+\chi_{k,l})^2(\mu_{S,k}^{1/2}+\chi_{S,k})^2N_S^2M_k^2,$$

$$\mathbb{E}[A_{k,R}] \approx 0.5M_kP_T\frac{\left(A_{k,r}A_{S,k}\left(\frac{d_{k,r}}{d_0}\right)^{-\zeta_{k,r}}\left(\frac{d_{S,k}}{d_0}\right)^{-\zeta_{S,k}}\right)}{(\mu_{k,r}+1)(\mu_{S,k}+1)} \times (\mu_{k,r}^{1/2}+\chi_{k,r})^2(\mu_{S,k}^{1/2}+\chi_{S,k})^2N_S^2M_k^2,$$

$$\mathbb{E}[B_{S,l}] \approx \frac{(L-1)P_T}{L}\frac{\left(A_{S,l}\left(\frac{d_{S,l}}{d_0}\right)^{-\zeta_{S,l}}\right)}{(\mu_{S,l}+1)}(\mu_{S,l}^{1/2}+\chi_{S,l})^2N_S^2 + \sum_{k=1}^{K}\frac{0.5M_kP_T(L-1)}{L}\frac{\left(A_{k,l}A_{S,k}\left(\frac{d_{k,l}}{d_0}\right)^{-\zeta_{k,l}}\left(\frac{d_{S,k}}{d_0}\right)^{-\zeta_{S,k}}\right)}{(\mu_{k,l}+1)(\mu_{S,k}+1)} \times (\mu_{k,l}^{1/2}+\chi_{k,l})^2(\mu_{S,k}^{1/2}+\chi_{S,k})^2N_S^2M_k^2,$$

$$\mathbb{E}[B_{k,R}] \approx \sum_{j=1}^{K}\frac{\left(A_{j,R}A_{S,j}\left(\frac{d_{j,R}}{d_0}\right)^{-\zeta_{j,R}}\left(\frac{d_{S,j}}{d_0}\right)^{-\zeta_{S,j}}\right)}{(\mu_{j,R}+1)(\mu_{S,j}+1)}(\mu_{j,R}^{1/2}+\chi_{j,R})^2(\mu_{S,j}^{1/2}+\chi_{S,j})^20.5M_j^3N_S^2P_T,$$

$$\mathbb{E}[C_{S,l}] \approx \sum_{k=1}^{K}\frac{\left(A_{k,l}A_{S,k}\left(\frac{d_{k,l}}{d_0}\right)^{-\zeta_{k,l}}\left(\frac{d_{S,k}}{d_0}\right)^{-\zeta_{S,k}}\right)}{(\mu_{k,l}+1)(\mu_{S,k}+1)}(\mu_{k,l}^{1/2}+\chi_{k,l})^2(\mu_{S,k}^{1/2}+\chi_{S,k})^20.5P_TN_S^2M_k^3,$$

$$\mathbb{E}[C_{k,R}] \approx P_T\frac{\left(A_{s,r}\left(\frac{d_{s,r}}{d_0}\right)^{-\zeta_{s,r}}\right)}{(\mu_{s,r}+1)}(\mu_{s,r}^{1/2}+\chi_{s,r})^2N_S^2 \text{ and}$$

$$\mathbb{E}[D_{k,R}] \approx \sum_{j\neq k}^{K}\frac{\left(A_{j,R}A_{S,j}\left(\frac{d_{j,R}}{d_0}\right)^{-\zeta_{j,R}}\left(\frac{d_{S,j}}{d_0}\right)^{-\zeta_{S,j}}\right)}{(\mu_{j,R}+1)(\mu_{S,j}+1)}(\mu_{j,R}^{1/2}+\chi_{j,R})^2(\mu_{S,j}^{1/2}+\chi_{S,j})^20.5M_j^3P_TN_S^2.$$

For the energy harvesting power available at the IRS, we have $\mathbb{E}[\hat{v}_{k,l}] \approx (A_{s,k}(d_{s,k}/d_0)^{-\zeta_{s,k}})^2/(\mu_{s,k}+1)^2P_T(1-\theta)^2M_k^6(\mu_{s,k}^{1/2}+\chi_{s,k})^4N_S^4$. Hence, the derivation and proof of the various SINR, rate and EH expectations is complete. ■

Appendix B
EE-WMMSE Based Solution

The optimal solutions for $\boldsymbol{\theta}_k$ and $\mathbf{v}_{S,l}$ are as follows.

A. IRS Reflection Coefficient Determination

From (6), the IRS harvests enough energy for circuit operation (i.e., $Q_k = P_{cir}$), $\boldsymbol{\theta}_k$ can be determined from EH constraint. First, let $\mathbf{x}_k = \{|(\mathbf{i}-\boldsymbol{\theta}_k)^{\frac{1}{2}H}\mathbf{G}_{S,k}\mathbf{v}_{S,1}|^4\}_1^L \in \mathbb{R}^{1\times L}$, and diagonal matrices $\mathbf{A}_k = \{\beta_k^2R_{At,k}^2/4R_{ld,k}\alpha_k^2V_{T,k}^2\}_1^L \in$

$\mathbb{R}^{L\times L}$, $\mathbf{B}_k = \{\beta_k^2 R_{At,k}^3/32R_{ld,k}\alpha_k^4 V_{T,k}^4\}_1^L \in \mathbb{R}^{L\times L}$ and $\mathbf{C}_k = \{\beta_k^2 R_{At,k}^4/1024R_{ld,k}\alpha_k^6 V_{T,k}^6\}_1^L \in \mathbb{R}^{L\times L}$. Then the EH constraint at equality is redefined as

$$0 = \mathbf{x}_k^{\frac{1}{2}}\mathbf{A}_k\mathbf{x}_k^{\frac{1}{2}} + \mathbf{x}_k^{\frac{3}{4}}\mathbf{B}_k\mathbf{x}_k^{\frac{3}{4}} + \mathbf{x}_k\mathbf{C}_k\mathbf{x}_k - P_{cir}. \tag{13}$$

$\mathbf{x}_k$ can be found from (13) with a root finding algorithm (e.g., Newton method). From the optimal $\mathbf{x}_k^\star$ solution, we have $\mathbf{x}_k^{\frac{1}{4}\star} = \mathcal{A}_k(\mathbf{i}-\boldsymbol{\theta}_k)^{\frac{1}{2}}$, where $\mathcal{A}_k = \{(\mathbf{G}_{S,k}\mathbf{v}_{S,1})^T\}_1^L$. Making $\boldsymbol{\theta}_k$ the subject; $(\mathbf{i}-\boldsymbol{\theta}_k)^{\frac{1}{2}} = \mathcal{A}_k^{-1}\mathbf{x}_k^{\frac{1}{4}\star}$, leading to $(\mathbf{i}-\boldsymbol{\theta}_k) = (\mathcal{A}_k^{-1}\mathbf{x}_k^{\frac{1}{4}\star})^T(\mathcal{A}_k^{-1}\mathbf{x}_k^{\frac{1}{4}\star})$. The optimal $\boldsymbol{\theta}_k^\star$ is given as

$$\boldsymbol{\theta}_k^\star = \mathbf{i} - (\mathcal{A}_k^{-1}\mathbf{x}_k^{\frac{1}{4}\star})^T(\mathcal{A}_k^{-1}\mathbf{x}_k^{\frac{1}{4}\star}). \tag{14}$$

B. PT Power Allocation Optimization

The EE WMMSE based problem is defined as

$$\underset{\{\mathbf{v}_{S,l}\}_{l=1}^L}{\text{minimize}}\ \hat{\Pi} - \hat{y}\mathcal{E} \text{ subject to (6b).} \tag{15}$$

Let $\Gamma = \hat{\Pi} - \hat{y}\mathcal{E}$. Now, the receive filters, weights and beamforming can easily be determined as follows [2].

The $\psi_{S,l}$ and $\psi_{k,l}$ filters are only found in the objective function. Hence, from $\partial\Gamma/\partial\psi_{S,l} = 0$ and $\partial\Gamma/\partial\psi_{k,R} = 0$ the closed-form solutions are found as

$$\begin{aligned}\psi_{S,l}^* &= E_{S,l}/[A_{S,l} + B_{S,l} + C_{S,l} + D_{S,l} + \sigma_l^2],\\ \psi_{k,R}^* &= E_{k,R}/[A_{k,R} + B_{k,R} + C_{k,R} + D_{k,R} + \sigma_R^2]\end{aligned} \tag{16}$$

by making $\psi_{S,l}$ and $\psi_{k,l}$ the subjects, respectively. The $\omega_{S,l}$ and $\omega_{k,R}$ are weights also determined from $\partial\Gamma/\partial\omega_{S,l} = 0$ and $\partial\Gamma/\partial\omega_{k,R} = 0$ respectively as

$$\begin{aligned}&\omega_{S,l} = (1/\varphi_{S,l}),\ \omega_{k,R} = (1/\varphi_{k,R}),\ \text{where}\\ &\varphi_{k,R} = |\psi_{k,R}|^2(A_{k,R} + B_{k,R} + C_{k,R} + D_{k,R} + \sigma_R^2) + 1\\ &- \psi_{k,R}E_{k,R},\ \text{and}\ \varphi_{S,l} = 1 - \psi_{S,l}E_{S,l} + |\psi_{S,l}|^2\\ &\times (A_{S,l} + B_{S,l} + C_{S,l} + D_{S,l} + \sigma_l^2).\end{aligned} \tag{17}$$

Now, differentiating the Lagrangian with respect to (w.r.t.) $\mathbf{v}_{S,l}$, equating it to zero and solving for $\mathbf{v}_{S,l}$, we derive

$$\mathbf{v}_{S,l} = (\boldsymbol{\Delta}_l)^{-1}\boldsymbol{\delta}_l, \tag{18}$$

where $\boldsymbol{\delta}_l = \sum_{k=1}^K \psi_{k,R}\omega_{k,R}(\mathbf{G}_{S,k}^H\boldsymbol{\Theta}_k^{\frac{1}{2}}\mathbf{g}_{k,R}) + \psi_{S,l}\omega_{S,l}(\mathbf{h}_{S,l} + \sum_{k=1}^K \mathbf{G}_{S,k}^H\boldsymbol{\Theta}_k^{\frac{1}{2}}\mathbf{g}_{k,l})$, $\boldsymbol{\Delta}_l = \sum_{j=1}^L |\psi_{S,j}|^2\omega_{S,j}\mathbf{h}_{S,j}\mathbf{h}_{S,j}^H - \hat{y} + 2\sum_{j=1}^L |\psi_{S,j}|^2\omega_{S,j}\sum_{k=1}^K(\mathbf{G}_{S,k}^H\boldsymbol{\Theta}_k^{\frac{1}{2}}\mathbf{g}_{k,j})(\mathbf{G}_{S,k}^H\boldsymbol{\Theta}_k^{\frac{1}{2}}\mathbf{g}_{k,j})^H + 2\sum_{k=1}^K\sum_{j=1}^K |\psi_{k,R}|^2\omega_{k,R}(\mathbf{G}_{S,j}^H\boldsymbol{\Theta}_j^{\frac{1}{2}}\mathbf{g}_{j,R}))(\mathbf{G}_{S,j}^H\boldsymbol{\Theta}_j^{\frac{1}{2}}\mathbf{g}_{j,R})^H + \mathbf{h}_{S,R}\mathbf{h}_{S,R}^H\sum_{j=1}^K |\psi_{j,R}|^2\omega_{j,R} - \lambda$. The Lagrangian w.r.t. $\mathbf{v}_{S,l}$ is given as $\mathcal{L}(\mathbf{v}_{S,l},\lambda) = \sum_{k=1}^K \omega_{k,R}|\psi_{k,R}|^2\sum_{l=1}^L |\mathbf{h}_{S,R}^H\mathbf{v}_{S,l}|^2 - \sum_{l=1}^L \omega_{S,l}\psi_{S,l}\Big(\mathbf{h}_{S,l}^H\mathbf{v}_{S,l} + \sum_{k=1}^K \mathbf{g}_{k,l}^H\boldsymbol{\Theta}_k^{\frac{1}{2}}\mathbf{G}_{S,k}\mathbf{v}_{S,l}\Big) - (\hat{y} + \lambda)\sum_{l=1}^L \|\mathbf{v}_{S,l}\|^2 - \sum_{k=1}^K \omega_{k,R}\psi_{k,R}\sum_{l=1}^L \mathbf{g}_{k,R}^H\boldsymbol{\Theta}_k^{\frac{1}{2}}\mathbf{G}_{S,k}\mathbf{v}_{S,l} + 2\sum_{k=1}^K \omega_{k,R}|\psi_{k,R}|^2\sum_{j=1}^K\sum_{l=1}^L |\mathbf{g}_{j,R}^H\boldsymbol{\Theta}_j^{\frac{1}{2}}\mathbf{G}_{S,j}\mathbf{v}_{S,l}|^2 + 2\sum_{l=1}^L \omega_{S,l}|\psi_{S,l}|^2\sum_{j=1}^L\sum_{k=1}^K |\mathbf{g}_{k,l}^H\boldsymbol{\Theta}_k^{\frac{1}{2}}\mathbf{G}_{S,k}\mathbf{v}_{S,j}|^2 + \sum_{l=1}^L \omega_{S,l}|\psi_{S,l}|^2\sum_{j=1}^L |\mathbf{h}_{S,l}^H\mathbf{v}_{S,j}|^2$.

From constraint (6b), $\mathbf{v}_{S,l}$ cannot exceed P_T. The derivation of λ is as follows. We multiply $\{\psi_{S,l},\psi_{k,R}\}$ solutions by their respective weights $\{\omega_{S,l},\omega_{k,R}\}$ to obtain $\{\psi_{S,l}\omega_{S,l}\}$ and $\{\psi_{k,R}\omega_{k,R}\}$. The two resulting expressions are merged (summed). The resulting equation from the merger is subtracted from the beamformer equation ($\mathbf{v}_{S,l}\times$(18)), and λ is made the subject, resulting in $\lambda = \frac{1}{P_T}(\sum_{l=1}^L |\psi_{S,l}|^2\sigma_l^2 + \sum_{k=1}^K |\psi_{k,R}|^2\sigma_R^2)$. $\boldsymbol{\Delta}_l$ is shown to be full-rank matrix as follows. Let $b = (\hat{y}+\lambda)$ and $\mathbf{B} = 2\sum_{j=1}^L |\psi_{S,j}|^2\omega_{S,j}\sum_{k=1}^K(\mathbf{G}_{S,k}^H\boldsymbol{\Theta}_k^{\frac{1}{2}}\mathbf{g}_{k,j})(\mathbf{G}_{S,k}^H\boldsymbol{\Theta}_k^{\frac{1}{2}}\mathbf{g}_{k,j})^H + \sum_{j=1}^L |\psi_{S,j}|^2\omega_{S,j}\mathbf{h}_{S,j}\mathbf{h}_{S,j}^H + \mathbf{h}_{S,R}\mathbf{h}_{S,R}^H\sum_{j=1}^K |\psi_{j,R}|^2\omega_{j,R} + 2\sum_{k=1}^K\sum_{j=1}^K |\psi_{j,R}|^2\omega_{j,R}(\mathbf{G}_{S,j}^H\boldsymbol{\Theta}_k^{\frac{1}{2}}\mathbf{g}_{j,R}))(\mathbf{G}_{S,k}^H\boldsymbol{\Theta}_k^{\frac{1}{2}}\mathbf{g}_{j,R})^H$. Then, the eigenvalue decomposition of the matrix $\boldsymbol{\Delta}_l$ is given by $\mathbf{U}_B(\Lambda_B - b\mathbf{I}_M)\mathbf{U}_B^H$. Obviously, $b > 0$ and the matrix $\mathbf{B}$ is a positive semi-definite matrix, therefore, $\boldsymbol{\Delta}_l$ is a full rank matrix [3], [13]. Also, the matrix $\boldsymbol{\Delta}_l$ is a non-zero matrix and the determinant of matrix B is not zero [3], [13].■

REFERENCES

[1] Y. Wang, M. Zhu, L. Li, Y. Liu, and E. Tong, "A review of reconfigurable intelligent surface assisted backscatter communication systems," in *Proc. IEEE Conf. Industrial Electronics and Applications*. Ningbo, China, Aug. 2023, pp. 1244–1249.

[2] D. K. P. Asiedu and J.-H. Yun, "Multiuser NOMA with multiple reconfigurable intelligent surfaces for backscatter communication in a symbiotic cognitive radio network," *IEEE Trans. Veh. Technol.*, vol. 72, no. 4, pp. 5300–5316, Apr. 2023.

[3] D. K. P. Asiedu, S. Mahama, C. Song, D. Kim, and K.-J. Lee, "Beamforming and resource allocation for multiuser full-duplex wireless-powered communications in IoT networks," *IEEE Int. Things J.*, vol. 7, no. 12, pp. 11 355–11 370, May 2020.

[4] S. Zhao, Y. Liu, S. Gong, B. Gu, R. Fan, and B. Lyu, "Computation offloading and beamforming optimization for energy minimization in wireless-powered irs-assisted MEC," *IEEE Internet Things J.*, pp. 19 466–19 478, Apr. 2023.

[5] H. Ma, H. Zhang, N. Zhang, J. Wang, N. Wang, and V. C. Leung, "Reconfigurable intelligent surface with energy harvesting assisted cooperative ambient backscatter communications," *IEEE Wireless Commun. Let.*, vol. 11, no. 6, pp. 1283–1287, Apr. 2022.

[6] S. Shen and B. Clerckx, "Beamforming optimization for MIMO wireless power transfer with nonlinear energy harvesting: RF combining versus DC combining," *IEEE Trans. Wireless Commun.*, vol. 20, no. 1, pp. 199–213, Sep. 2020.

[7] S. Wang, J. Xu, and Y. Zeng, "On the energy-efficiency trade-off between active and passive communications with RIS-based symbiotic radio," *arXiv preprint arXiv:2305.13621*, May 2023.

[8] X. Ding, Q. Zhang, Y.-C. Liang, and Y. Pei, "Reconfigurable intelligent surface design for symbiotic radio system through BER minimization," in *Proc. IEEE Int. Conf. Commun. Workshops*. Seoul, South Korea, May 2022, pp. 764–769.

[9] H. Peng, C.-Y. Ho, Y.-T. Lin, and L.-C. Wang, "Energy-efficient symbiotic radio using generalized benders decomposition," in *Proc. IEEE Veh. Technol. Conf.* London, United Kingdom, Sep. 2022, pp. 1–5.

[10] D. K. P. Asiedu and J.-H. Yun, "Full-duplex multiuser wireless information and power transfer with a multistage nonlinear rectifier energy harvesting model," *IEEE Wireless Communications Letters*, Jan. 2024.

[11] K. Shen and W. Yu, "Fractional programming for communication systems — Part I: Power control and beamforming," *IEEE Trans. Signal Process.*, vol. 66, no. 10, pp. 2616–2630, Mar. 2018.

[12] L. You, J. Xiong, X. Yi, J. Wang, W. Wang, and X. Gao, "Energy efficiency optimization for downlink massive MIMO with statistical CSIT," *IEEE Trans. Wireless Commun.*, vol. 19, no. 4, pp. 2684–2698, Jan. 2020.

[13] M. C. Vanderveen, A.-J. Van der Veen, and A. Paulraj, "Estimation of multipath parameters in wireless communications," *IEEE trans. signal process.*, vol. 46, no. 3, pp. 682–690, Mar. 1998.